WIND SPEED GRADIENTS AND WAKES MAPPED USING SAR FOR A STUDY AREA IN SOUTH-EAST CHINA

Abdalmenem Owda, Merete Badger

DTU Wind and Energy Systems – Technical University of Denmark
Risø Campus, Frederiksborgvej 399
Roskilde, DK-4000

ABSTRACT

The rapid increase of offshore wind installations in the south-China sea near the coast triggers a new demand for studying the effects of horizontal wind speed gradients and the wind power variation within the coastal zone. The advent of Synthetic Aperture Radar (SAR) data offers an opportunity to map wind speed gradients and wind farm wakes with high spatial resolution. We have retrieved wind maps at 10 m above mean sea level (m.s.l.) from Sentinel-1 SAR and Envisat Advanced SAR observations. Generally, the speed of the prevailing south-easterly winds and wind power declined about 8% and 22%, respectively. Although the southern offshore wind farms (OWFs) were not in operation before December 2019, the wind velocity deficit at the upstream side of northern OWFs were between 8-12 %. After the southern OWFs became online, the region between OWFs is subjected to wind wakes and coastal upwelling effects. The coastal upwelling phenomena speeds up the wind at the downstream sides of OWFs that reduce the wind wakes up to 8-10%. The wind wakes extended 20 km beyond the southern OWFs.

Index Terms— SAR, wind speed gradients, wind wakes, offshore wind farms.

1. INTRODUCTION

China has overtaken Germany as the worlds' no.2 offshore wind energy market in cumulative installations with 3060 MW in 2021. Furthermore, China is expected to overtake the UK and have the largest amount of offshore wind power installed globally by the end of 2021. China will hit 28.3% and be followed by the UK 21.9% of global offshore cumulative installations, according to the most recent Global Wind Energy Council (GWEC)'s report in 2021 [1]. The northwestern part of the south China sea has developed into a rich source of wind energy for China. Most of the Chinese offshore installations are adjacent to each other and to the coastline. The rapid increase of the offshore installations in the area is highlighting the need to observe the offshore wind conditions in the coastal zone.

A Synthetic Aperture Radar (SAR) is a side-looking satellite sensor, which can be used to visualize the fine spatial details of the wind flow close to the coast. SAR observations have been utilized for a wide range of applications ranging from wind resource assessments [2], identifying offshore wind farm wakes and coastal wind speed gradients [3]. Several studies have validated the wind speeds retrieved from SAR observations with respect to other datasets and typically found the root mean square error to be less than 2 m/s. Ahsbahs et al. show good agreement through comparison of 15 Sentinel-1A wind maps against light detection and ranging (LiDAR) measurements at the west coast of Denmark [4].

Wind wakes are defined as areas of reduced wind speed at the downstream side of the offshore wind farms (OWFs) because of energy extraction by the wind turbines. Wakes can extend several tens of kilometers, therefore, the wakes can interact with adjacent OWFs and have severe consequences for the power production, as the wind power is proportional to the cube of the wind speed.

The wind speed within the coastal zone is also affected by (i) the surface discontinuity at the coastline, (ii) the influence of onshore topography, and (iii) thermal gradients [5]. The magnitude of wind velocity deficits at the downstream side of OWFs is thus a combination of wind wakes and the effects of horizontal coastal wind speed gradients. Hasager et al. concluded that the winds in the coastal zones have larger spatial gradients than further offshore and many other wind phenomena occur in coastal zones [6]. Owda et al. have studied the effects of coastal gradients for many OWFs in northern European seas and found strong gradients inversely proportional with the distance to shore. They decomposed the wind gradient effects from wind wakes based on SAR observations before commissioning of the OWFs [3].

The aim of the present study is to map the horizontal speed gradients for a coastal area with several OWFs at the southeastern coast of China. Furthermore, to illustrate the effects of the coastal wind speed gradients on the potential wind power production. Characterizing the spatial wind variability can be used to support different aspects of OWFs planning in this area. A description of the data and methods is presented in Section 2. Results are shown in Section 3. Finally, a discussion and main conclusions are recapped in Section 4.

2. DATA AND METHODS

2.1. Data

2.1.1. Sentinel 1A/B & Envisat

Sentinel 1A/B is a constellation of two different satellites, Sentinel-1A (2014-present) and Sentinel-1B (2016-2021), sharing the same orbital plane at the mean altitude 693 km. Envisat (2002-2012) carried an Advanced Synthetic Aperture Radar (ASAR) instrument at the altitude 800 km. The satellite data were acquired using C-band SAR sensors operating at 5.405 GHz. The satellites are in a near-polar, sun-synchronous orbit with a 6 and 35 day repeat cycle for the Sentinel-1 constellation and Envisat, respectively. In this study, VV co-polarized images with extra wide (EW) for Sentinel-1 and wide swath mode for Envisat were used.

2.2. Study area

Our study area is in southeast China and at 120 to 120.8 longitude and 34 to 34.6 latitude. The area has four OWFs (Figure 1). Table I presents the characteristics of each OWF. Table II presents available SAR scenes based on commissioning date of first operated southern OWFs (Datang Binhai). We refer *southern OWFs* term to Datang Binhat and Spic Binhat South H3 and *northern OWFs* term to SPIC Binhai North H1 and H2.

TABLE I. OFFSHORE WIND FARMS' CHARACTERISTICS

OWF	Commissioning date	Capacity (MW)	Turbines
SPIC Binhai North H1	6 June 2016	100	25
SPIC Binhai North H2	30 June 2018	400	100
Datang Binhai	25 December 2019	300	95
SPIC Binhai South H3	18 January 2021	300	75

TABLE II. AVAILABLE SAR SCENES BEFORE AND AFTER 25TH DECEMBER 2019 FOR THE INVESTIGATED PERIOD FROM 2000 TO 2021

From	To	Number of scenes
01 January 2000	25 December 2019	49
25 December 2019	31 December 2021	37

2.3. Methods

2.3.1. SAR wind retrieval

The SAR radar observables relate to the local near-surface wind speed using an empirical equation called a geophysical model function (GMF)[7]. We have used the GMF version CMOD5.N; it relates the roughness components of the ocean surface, the radar incident angle, and the wind direction relative to antenna look direction with the sea surface wind at 10 m above m.s.l. (***U***). The SAR wind data are projected to geographic coordinates with a regular grid spacing of 0.5 km. Owda et al. have explained the processing of SAR scenes to wind maps in detail [3].

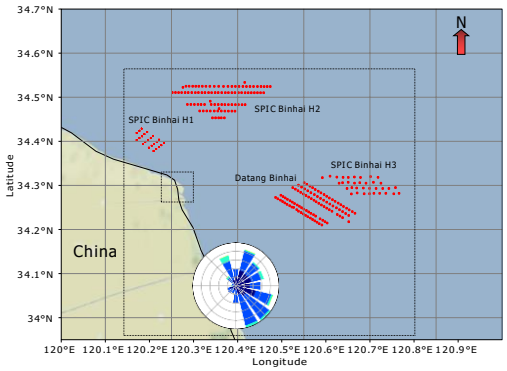

Fig. 1. The study area has four OWFs. The big black dashed rectangle refers to the dimension of the grid used for the SAR wind analysis. Small, dashed rectangle refers to an area with mixed features (man-made, sand banks or mud flats). Wind rose refers to the wind direction which is taken from the global forecasting model for the scenes in Table II.

2.3.2 Mean wind speed, deficit and power variation calculation

A grid of 60×50 km is overlaid over the entire study area and used to retrieve SAR wind measurements with the regular grid spacing 1.5 km between each rectangular bin inside the grid. Figure 1 illustrates the boundary of the used grid. Based on the 86 available SAR scenes, the wind rose for a point close to the coast shows that the prevailing wind direction is from the southeast. In this study, we have taken in our analysis only the scenes with wind directions between 90 and 180 degrees "southeast". The mean wind speed (U) is computed for our area of interest based on the selected scenes of each period in Table II. Furthermore, the relative wind speed difference to the mean upstream wind (ΔU) is calculated for the entire grid. The wind power density (P) is estimated using a simple power equation. Equations 1, 2 refer to ΔU *(%)* and *P (Watt/m^2)*, respectively.

$$\%\Delta U = \frac{U_{upstream} - U_{grid,x}}{U_{upstream,x}} \times 100 \quad (1)$$

where $U_{upstream}$ is the upstream velocity and $U_{grid,x}$ is the mean wind speed of the rectangular bin x in the grid. A positive ΔU indicates an area with reduced wind speed and

$$P_{mean} = \frac{1}{2} \times \rho \times \overline{U}^3 \quad (2)$$

where ρ is the air density (1.255 kg/m^3) and $\overline{U}^3$ is the mean of the cubed velocity series of each rectangular bin in the grid.

3. RESULTS

3.1. Before southern OWFs commissioning

Figure 2 illustrates the results of processing scenes of the study area with southeasterly winds before 25 December 2019. Figure 2a shows the mean wind speed variation.

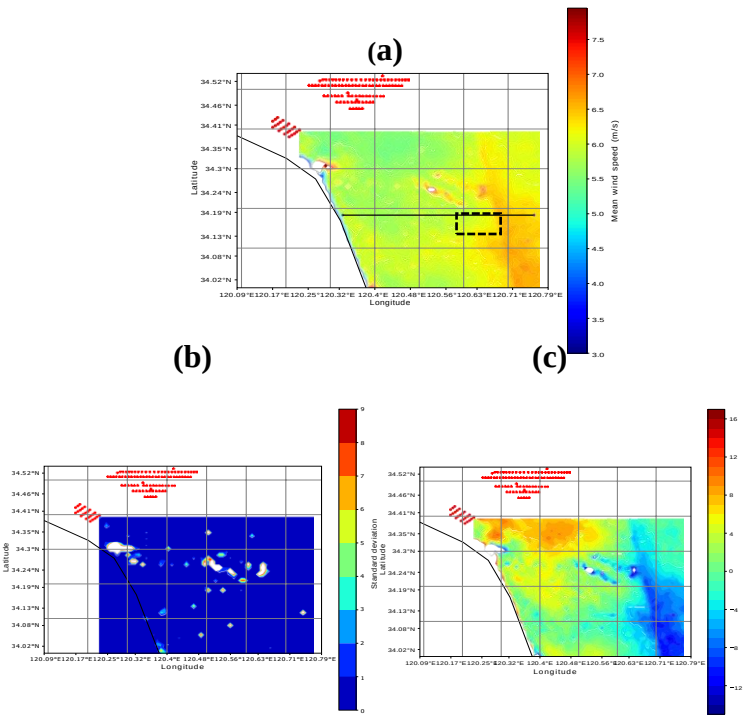

Fig. 2. Results before southern OWF commissioning: (a) mean wind speed, (b) standard deviation of the mean wind speed map, and (c) wind velocity deficit with respect to the mean upstream value from the black dashed rectangle in (a).

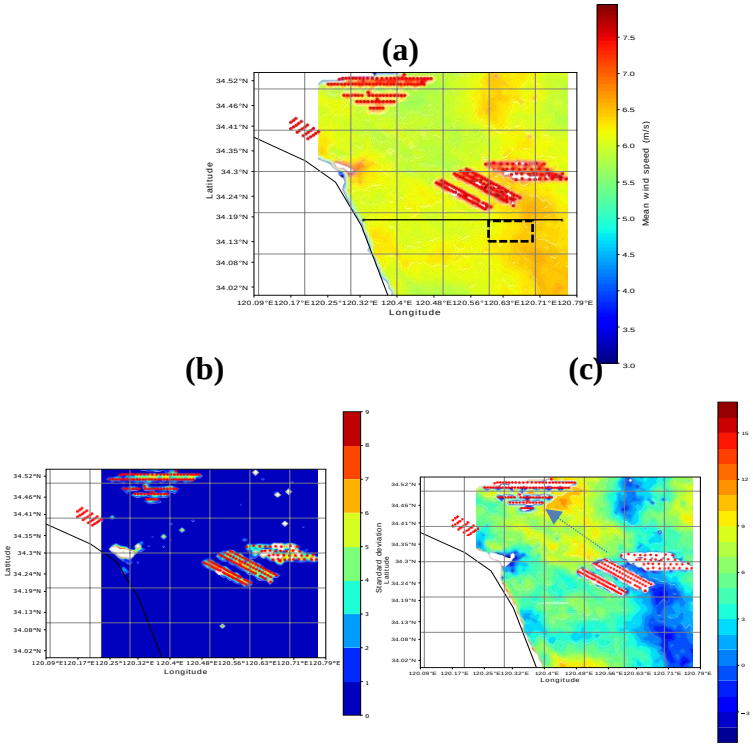

Fig. 3. Same as Figure 2 but after the commissioning of OWFs.

The highest wind speed values were observed at the lower right corner with 6.5-7 m/s (fit well with the global wind atlas map of the area at 10 m.s.l, https://globalwindatlas.info/). For this period, the results above the latitude 34.41 are clipped from the plot because few overlapped SAR scenes exist. Figure 2b illustrates the corresponding standard deviation values of the Figure 2a, it shows that the dominant standard deviation values are lower than 1 m/s. However, some high standard deviation values can be observed in the grid, which probably belongs to man-made objects, and the white mask areas belong to an area mixed with man-made objects, sand banks and wind parks construction areas. Figure 2c shows the mean velocity deficit percentile, which is computed for the whole grid based on the mean upstream value in the black dashed rectangle in front of the proposed location of the southern OWFs. Even though the southern OWFs were not in service, there is a significant amount of wind reduction, about 8-12% of upstream wind in areas close to the northern OWFs.

3.2. After southern OWFs commissioning

After 25th December 2019 the southern OWFs were in operation. Figure 3a shows the mean wind speed variation and it is like the wind speed variation before commissioning (see Figure 2a). Figure 3b illustrates that the dominant standard deviation values of the mean wind speed values are less than 1 m/s with exceptions for random man-made objects and wind parks areas. Figure 3c shows the southern OWFs' wind wakes interaction with northern OWFs.

The wind wake streaks (blue dashed arrow) are extended far beyond southern to northern OWFs (20 km) with a range of wind deficit 8-10 %. Surprisingly, the first period shows higher wind deficit values compared with the second period. The manual inspection of the SAR scenes of period two shows about 25% of the processed scenes have coastal upwelling effects compared with 5% for the first period (Figure 4b shows one example of these scenes). The wind speed increased in the northwestern part of the area of interest near the coast that mitigated the values of velocity deficits.

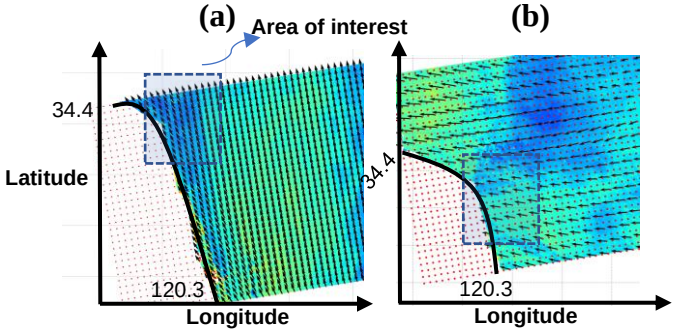

Fig. 4. SAR wind map of a processed SAR scene S1A for our area of interest at acquisition time (a) 9th April 2021 09:55:34 and (b) 30th May 2021 21:22:43.

3.2. Mean wind speed and power variation along a transect line

Figure 5 demonstrates the variation of wind speed along a 32 km long transect line south of southern OWFs (black solid line in Figure 2a & 3a); to avoid any wind wake effects from

the OWFs. For all processed periods, the wind speed decreased gradually along the transect line up to a few kilometers from the coast. Figure 5 exposes about 8% wind deficit over the 32 km distance (0.24 m/s per km). As a result of that, the power losses on the same transect line reaches to 22 %.

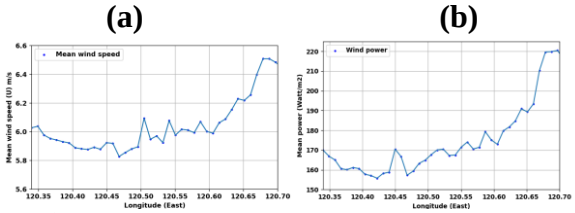

Fig. 5. (a) Average mean wind speed (m/s) and (b) power variation (Watt/m^2).

4. CONCLUSION

This paper demonstrates how the spatial variation of the wind speed is strong near the curved coast. It also shows the effects of natural wind speed gradients on the wind power potential. The high spatial resolution of SAR can provide valuable information about the wind speed variation from far offshore to the coastal zone. The results have shown strong coastal gradients as the winds approach the coastline. Along a transect line at the southern region of the area investigated, it shows the speed is reduced about 8 % over the 32 km distance. In terms of wind power estimation, the power reduction along the same transect line is about 22%. The region between the southern and northern OWFs within our area of interest is subject to different wind velocity deficits before and after commissioning southern OWFs. The wind deficit values before commissioning (see Figure 2c) are bigger than after commissioning (see Figure 3c). That refers to the high wind speed values at the northwestern corner of the study area from some easterly winds' scenes. For the southerly winds, the land blocked the wind flow nearby, (Figure 4a is an example), therefore, there is significant different on wind speed between the right and left side of wind speed maps for both investigated periods (see Figure 2 and 3 a). The coastal areas in this region experienced a strong combination of coastal upwelling [8] and wind speed gradient effects. Recent commissioning dates of the southern OWFs limit the number of samples that we can obtain. Additionally, found that for an area mixed with different features (like sand banks, mud flats) can lead to high standard deviation in mean wind speed, which are not wind induced. For wind energy applications, while 10 m winds are not directly applicable for offshore wind energy application, various methods can be used to extrapolate our results to the hub height of wind turbines [9]. The SAR wind maps used in this study are publicly available [10].

5. ACKNOLEDGEMENTS

The PhD of main author Abdalmenem Owda is funded by the European Union Horizon 2020 research and innovation program under grant agreement no. 861291 as part of the Train2Wind Marie Skłodowska-Curie Innovation Training Network (https://www.train2wind.eu/). Travel support has been granted through the ESA DRAGON5 project Remote Sensing of Changing Coastal Marine Environments (ReSCCoME), ID.57192.

6. REFERENCES

[1] J. Lee and F. Zhao, "Global Wind Report 2021," *Global Wind Energy Council*, pp. 1–80, 2021, [Online]. Available: http://www.gwec.net/global-figures/wind-energy-global-status/.

[2] C. B. Hasager, P. Astrup, M. B. Christiansen, M. Nielsen, and R. Barthelmie, "Wind resources and wind farm wake effects offshore observed from satellite," in *European Wind Energy Conference and Exhibition 2006, EWEC 2006*, 2006, vol. 1.

[3] A. Owda and M. Badger, "Wind Speed Variation Mapped Using SAR before and after Commissioning Date of Offshore Wind Farms," pp. 1–27, 2022.

[4] T. Ahsbahs, M. Badger, I. Karagali, and X. G. Larsén, "Validation of sentinel-1A SAR coastal wind speeds against scanning LiDAR," *Remote Sensing*, vol. 9, no. 6, pp. 1–17, 2017, doi: 10.3390/rs9060552.

[5] R. J. Barthelmie, J. Badger, S. C. Pryor, C. B. Hasager, M. B. Christiansen, and B. H. Jørgensen, "Offshore coastal wind speed gradients: Issues for the design and development of large offshore windfarms," *Wind Engineering*, vol. 31, no. 6, pp. 369–382, 2007, doi: 10.1260/030952407784079762.

[6] C. B. Hasager, "Offshore winds mapped from satellite remote sensing," *Wiley Interdisciplinary Reviews: Energy and Environment*, vol. 3, no. 6, 2014, doi: 10.1002/wene.123.

[7] H. Hersbach, A. Stoffelen, and S. De Haan, "An improved C-band scatterometer ocean geophysical model function: CMOD5," *Journal of Geophysical Research: Oceans*, vol. 112, no. 3, pp. 1–18, 2007, doi: 10.1029/2006JC003743.

[8] X. Li, W. Pichel, and X. Yang, "Spaceborne SAR imaging of coastal ocean phenomena," *IEEE Geoscience and Remote Sensing Letters*, no. 20, pp. 36–38, 1979.

[9] C. B. Hasager *et al.*, "Study on offshore wind farm wakes based on Envisat ASAR, Radarsat-2 and Sentinel-1," 2016.

[10] Badger, Merete; Karagali, Ioanna; Cavar, Dalibor (2022): Offshore wind fields in near-real-time. Technical University of Denmark. Dataset. https://doi.org/10.11583/DTU.19704883.v1